Supplement of Atmos. Meas. Tech., 18, 1561–1589, 2025
https://doi.org/10.5194/amt-18-1561-2025-supplement

Atmospheric Measurement Techniques
Open Access
EGU

Supplement of

Global retrieval of TROPOMI tropospheric HCHO and NO_2 columns with improved consistency based on the updated Peking University OMI NO_2 algorithm

Yuhang Zhang et al.

Correspondence to: Jintai Lin (linjt@pku.edu.cn) and Michel Van Roozendael (michel.vanroozendael@aeronomie.be)

Table S1. Specifics for the HCHO and NO_2 SCD retrieval of TROPOMI operational products.

Parameter	HCHO (v2.4.1)	NO_2 (v2.4.0)
Type of DOAS fit	Optical fit	Intensity fit
Fitting interval	328.5-359 nm	405-465 nm
Absorption cross sections	HCHO, Meller and Moortgat (2000), 298 K NO_2, Vandaele et al., (1998), 220 K O_3, Serdyuchenko et al. (2014), 223 + 243 K BrO, Fleischmann et al. (2004), 223 K O_2-O_2, Thalman and Volkamer (2013), 293 K Ring effect, Chance and Spurr (1997) Non-linear O_3 absorption effect, Puķīte et al. (2010)	NO_2, Vandaele et al. (1998), 220 K O_3, Serdyuchenko et al. (2014), 243 K O_2-O_2, Thalman and Volkamer (2013), 293 K H_2O_{vap} based on HITRAN 2012 data (Van Geffen et al., 2015) H_2O_{liq}, Pope and Fry (1997) Ring effect, Chance and Spurr (1997)
Slit function	Pre Flight Model	Pre Flight Model
Polynomial	5th order	5th order
Intensity offset correction	Linear offset	Currently turned off
Reference spectrum I_0	Average of radiances, per row, selected in the equatorial Pacific within the last 5 valid days	Daily measured solar spectrum from TROPOMI
High-resolution solar irradiance spectrum for wavelength calibration	Chance and Kurucz (2010)	Chance and Kurucz (2010)

Table S2. Comparison of the specifications between GEOS-CF and TM5-MP.

Specification	GEOS-CF (Keller et al., 2021)	TM5-MP (Huijnen et al., 2010; Williams et al., 2017)
Resolution	Horizontal: 0.25° × 0.25° Vertical: 72 hybrid-eta levels	Horizonal: 1° × 1° Vertical: 34 layers
Meteorological field	GEOS-FP for instrument teams (GEOS FP-IT; https://gmao.gsfc.nasa.gov/pubs/docs/Lucchesi865.pdf)	ERA-Interim re-analysis (Dee et al., 2011)
NO_x & VOC emissions	(1) Anthropogenic: HTAP v2.2 (Janssens-Maenhout et al., 2015); RETRO (Schultz et al., 2008); DICE-Africa (Marais and Wiedinmyer, 2016) (2) Aircraft: AEIC Stettler et al. (2011) (3) Biomass burning: QFED v2.5 (https://ntrs.nasa.gov/citations/20180005253) (4) Lightning NO_x: Murray et al. (2012) (5) Soil NO_x: Hudman et al. (2012) (6) Biogenic VOCs: MEGAN v2.1 (Guenther et al., 2012)	(1) Anthropogenic: MACCity (Granier et al., 2011) (2) Aircraft (only for NO): a homogeneous hourly flux estimate (3) Biomass burning: GFED v3 (van der Werf et al., 2010) (4) Lightning NO_x: parameterization using convective precipitation fields (Meijer et al., 2001) with the constraint on the annual global emission term at ~ 6Tg N yr^{-1} (5) Biogenic component: CLM-MEGAN v2.1 (Zeng et al., 2015); MEGAN (Sindelarova et al., 2014)
Chemistry	(1) Full tropospheric chemistry for NOx + HOx + VOC + O_3 + halogen + aerosols (https://wiki.seas.harvard.edu/geos-chem/index.php?title=Simulations_using_KPP-built_mechanisms) (2) Stratospheric chemistry fully coupled with the tropospheric chemistry through the Unified tropospheric-stratospheric Chemistry eXtension (UCX; Eastham et al., 2014)	(1) Modified CB05 (mCB05) chemical mechanism for gas-phase chemistry (Williams et al., 2013) (2) No aerosol scheme (3) no explicit stratospheric chemistry
Advection scheme	Finite-volume dynamical core (Lin, 2004) with a cubed sphere grid discretization (Putman and Lin, 2007)	Slopes scheme (Russell and Lerner, 1981)

Convection Scheme	Relaxed Arakawa-Schubert scheme (Moorthi and Suarez, 1992)	Convective mass fluxes and detrainment rates from the ERA-Interim re-analysis (Dee et al., 2011)
Boundary layer diffusion	Non-local Lock scheme (Lock et al., 2000) interfaced with the Richardson-number-based scheme of Louis and Geleyn (J-F. Louis et al., 1982)	Holtslag and Boville (1993)

Table S3. Statistics of separate validation results against ground-based MAX-DOAS and PGN measurements.

HCHO	MAX-DOAS		PGN	
	POMINO	RPRO	POMINO	RPRO
Slope	0.54	0.62	0.57	0.61
Offset [10^{15} molec.cm^{-2}]	2.19	0.37	0.79	0.22
Correlation	0.68	0.70	0.61	0.66
NMB	−26.3%	−32.3%	−31.7%	−35.6%

NO_2	MAX-DOAS		PGN	
	POMINO	RPRO	POMINO	RPRO
Slope	0.65	0.58	0.77	0.69
Offset [10^{15} molec.cm^{-2}]	0.77	0.70	0.70	0.81
Correlation	0.83	0.85	0.84	0.86
NMB	−17.5%	−27.8%	−5.3%	−14.9%

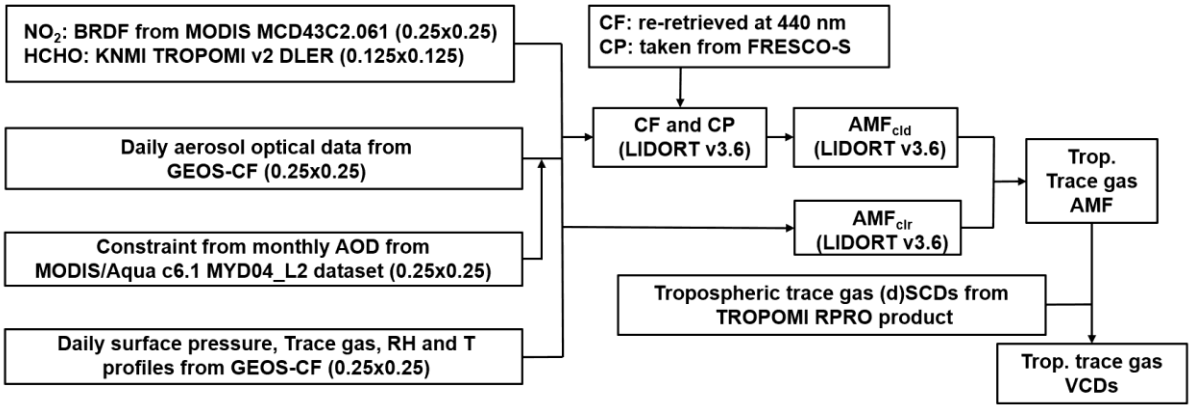

Figure S1. Flow chart of global POMINO-TROPOMI algorithm for consistent HCHO and NO_2 AMF calculation.

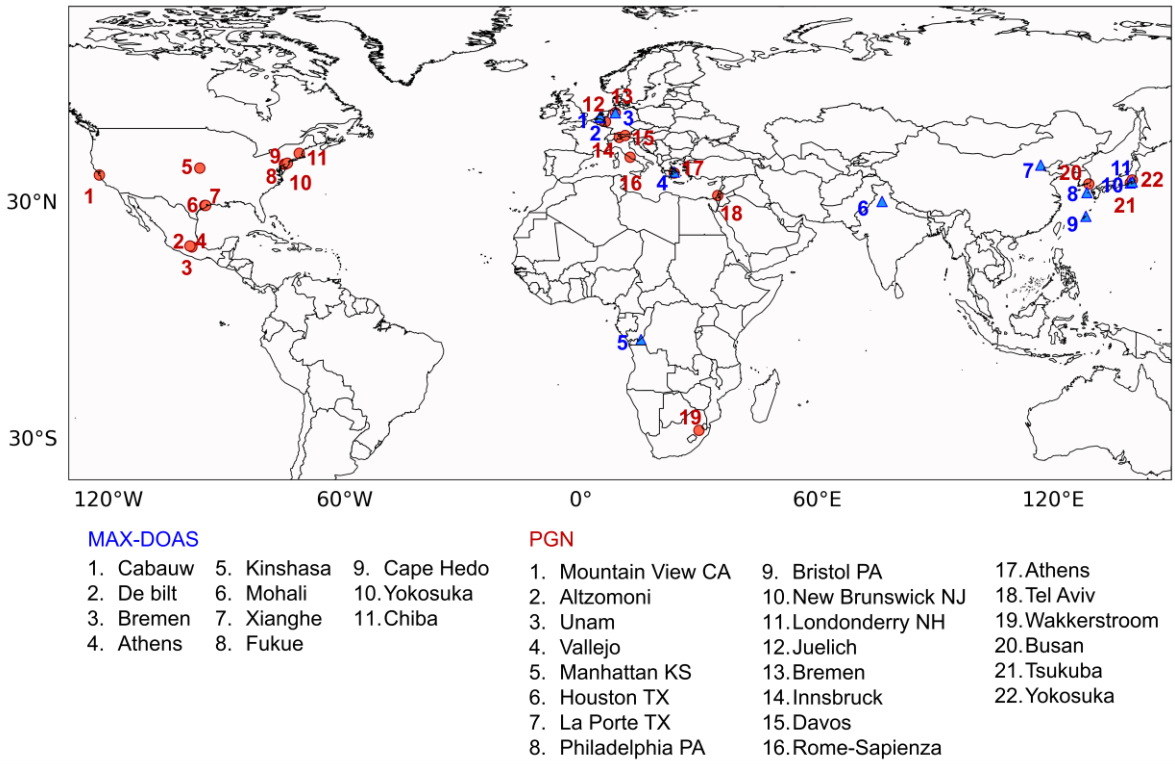

Figure S2. Spatial distribution of ground-based MAX-DOAS and PGN sites selected for validation in this study.

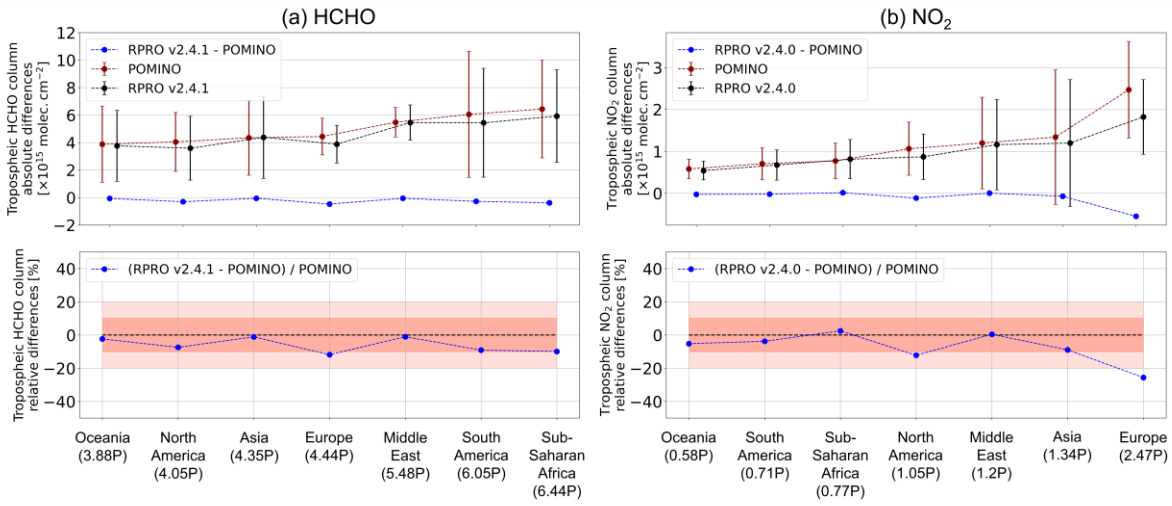

Figure S3. Absolute and relative differences between POMINO and RPRO (**a**) HCHO and (**b**) NO_2 tropospheric columns averaged in April, July, October 2021, and January 2022 in seven regions. Regions are sorted as a function of POMINO mean HCHO or NO_2 columns, with values (in the unit of "P" as Pmolec.cm^{-2} = 1 × 10^{15} molec.cm^{-2}) shown in the brackets in the bottom axis. Mean POMINO (red) and RPRO (black) columns are also plotted with the absolute differences in the upper panel. Error bars represent the standard deviations of the columns. Pink areas indicate 10% and 20% relative differences.

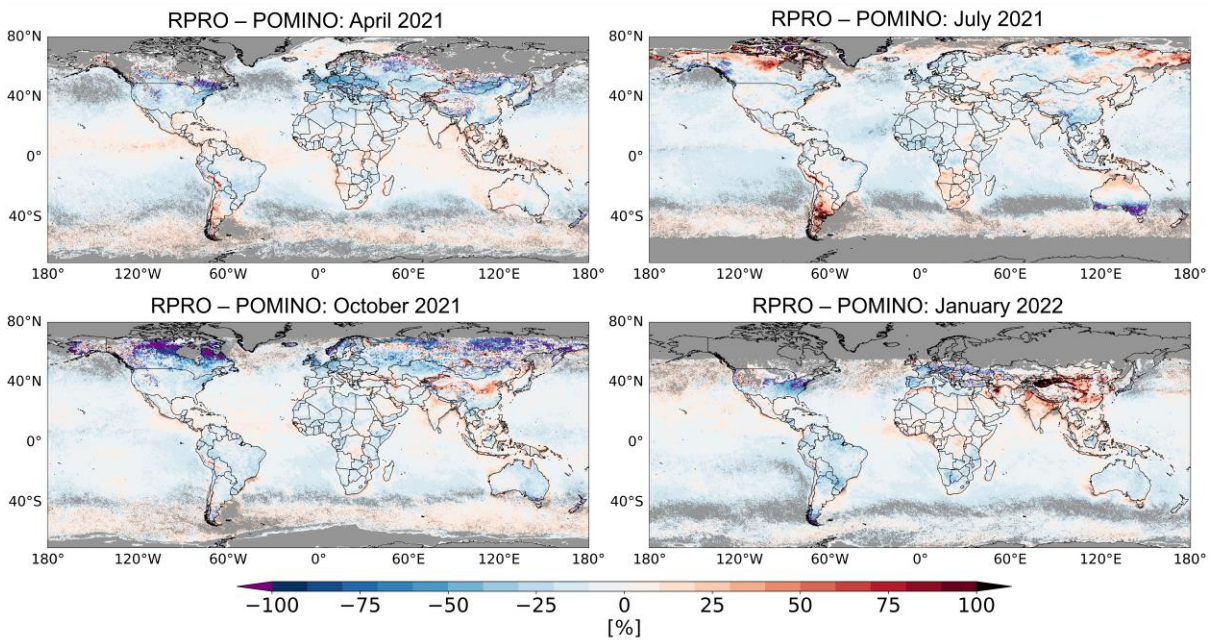

Figure S4. Relative differences of tropospheric HCHO columns of RPRO to POMINO in April 2021, July, October 2021 and January 2022. The regions in gray mean that there are no valid observations.

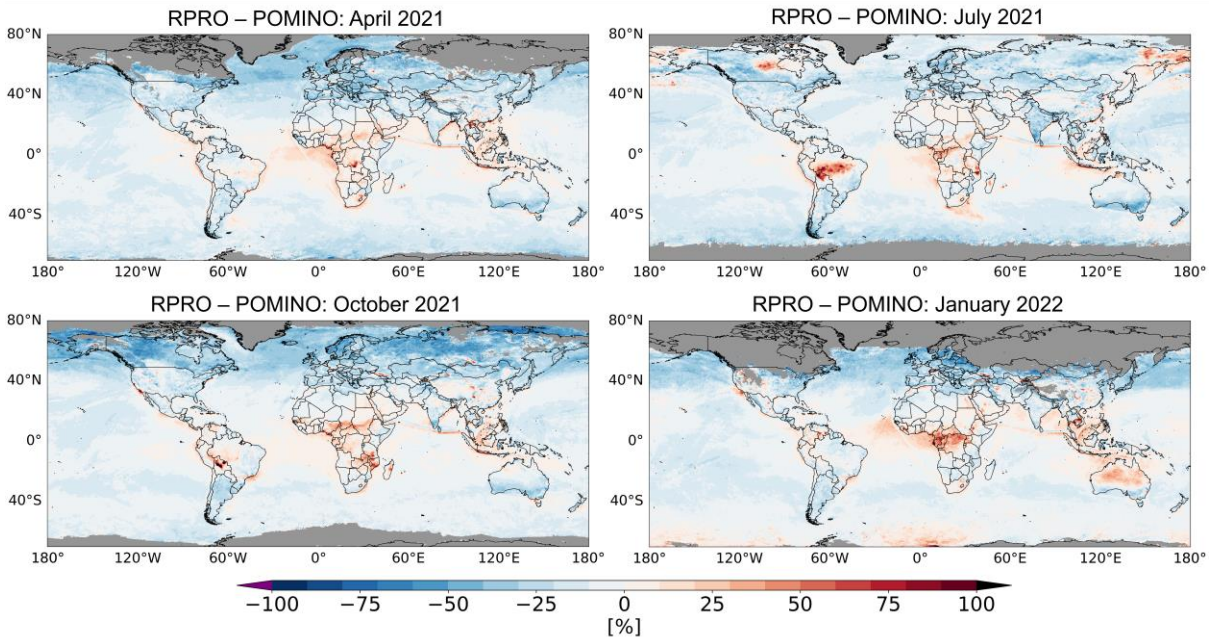

Figure S5. Similar to Figure S4 but for NO_2.

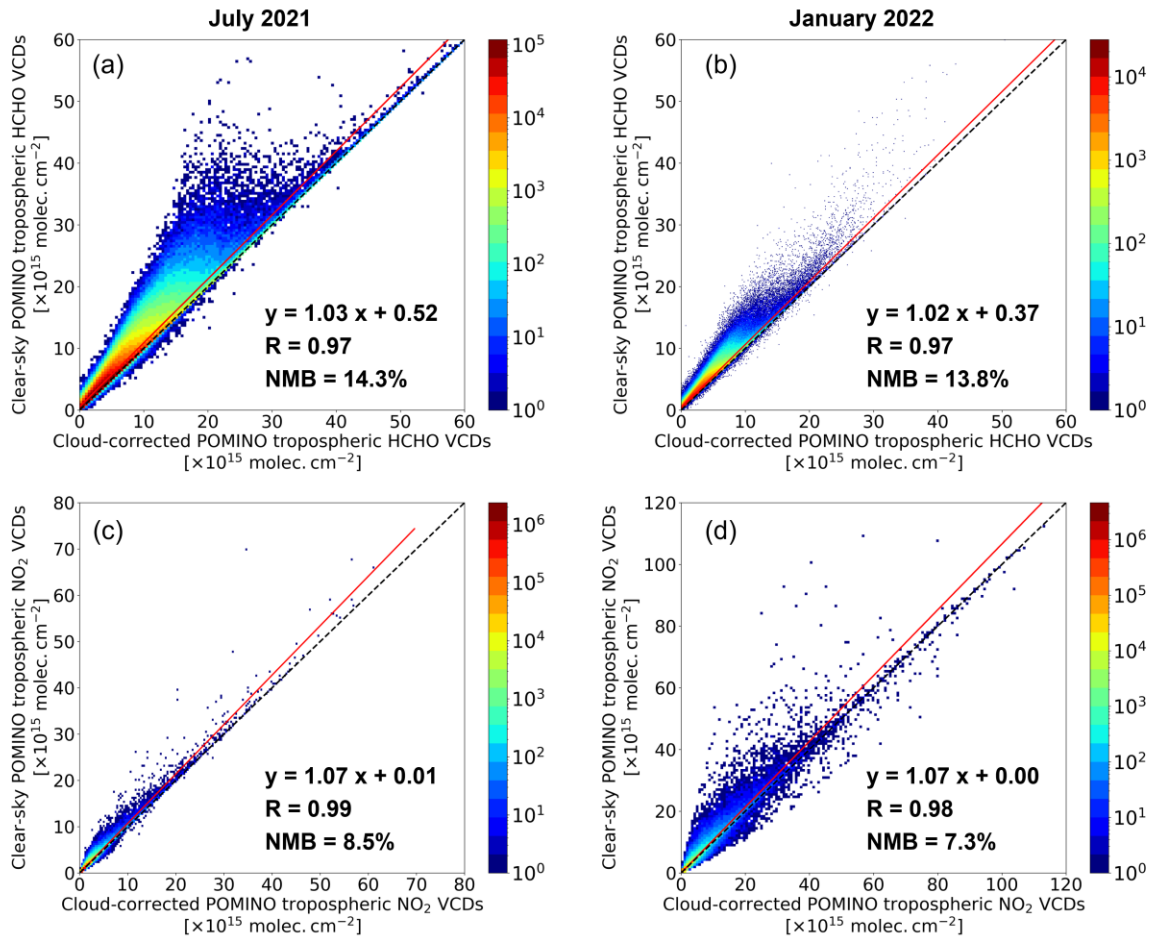

Figure S6. Scatterplots of POMINO tropospheric HCHO (**a** and **b**) and NO2 (**c** and **d**) VCDs retrieved using either aerosol-corrected and cloud-corrected total AMF (x-axis) or aerosol-corrected clear-sky AMF (y-axis), from all pixels where the difference between surface pressure and FRESCO-S cloud top pressure is equal to 100 hPa or less. The left column shows the results for July 2021, and the right column for January 2022. The slope, offset and correlation from a linear regression using the robust Theil-Sen estimator and normalized mean bias (NMB) are given in each panel and plotted as the red line. The black dashed line is the 1:1 line.

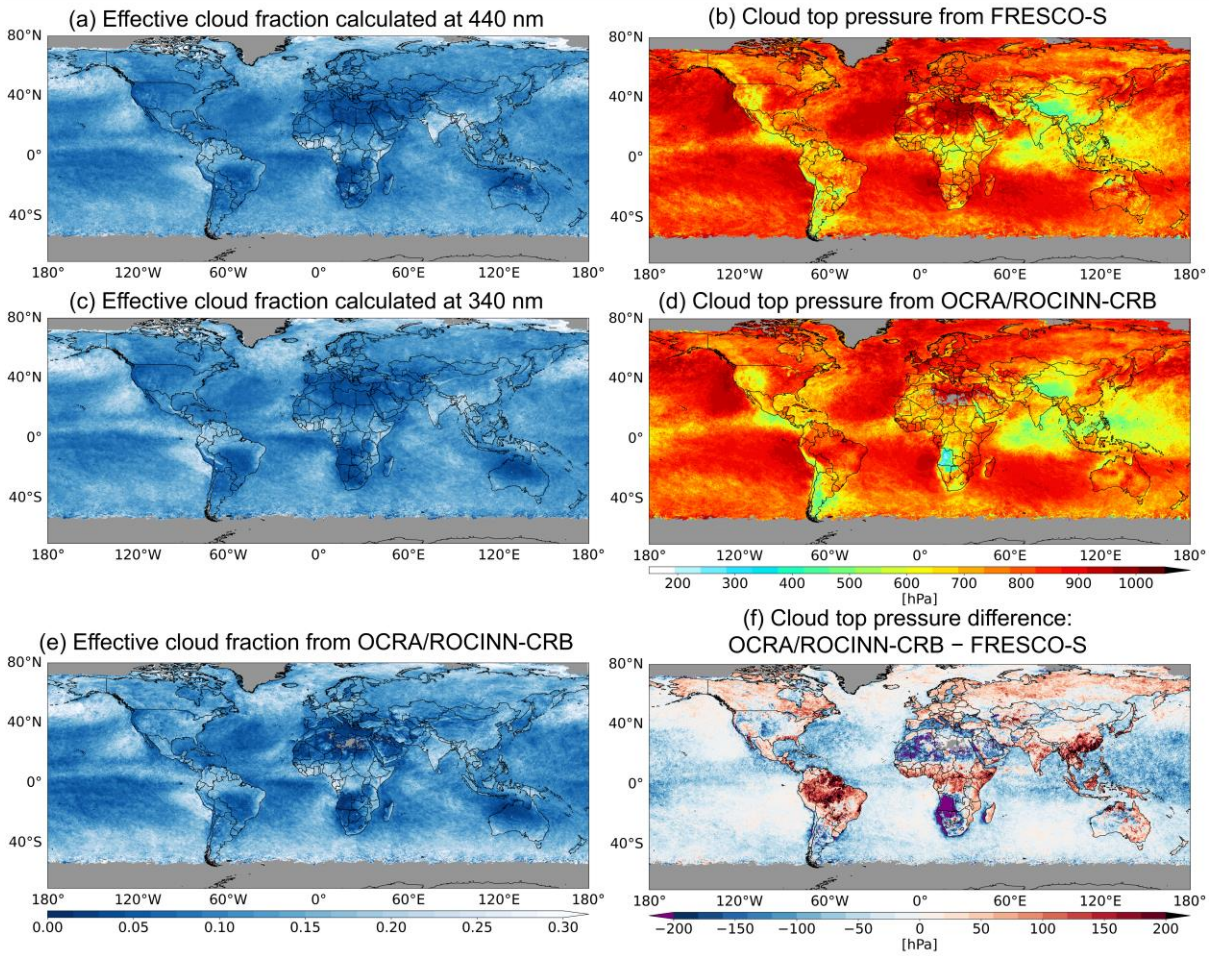

Figure S7. Comparison of cloud parameters used for sensitivity tests in July 2021. (**a**) POMINO-based effective cloud fraction calculated at 440 nm; (**b**) cloud top pressure from FRESCO-S product; (**c**) POMINO-based effective cloud fraction calculated at 340 nm; (**d**) cloud top pressure from OCRA/ROCINN-CRB product; (**e**) effective cloud fraction from OCRA/ROCINN-CRB product and (**f**) difference of (**d**) to (**b**). Pixels with HCHO QA > 0.5 and ECF of each case > 0.01 are included. The regions in gray mean that there are no valid observations.

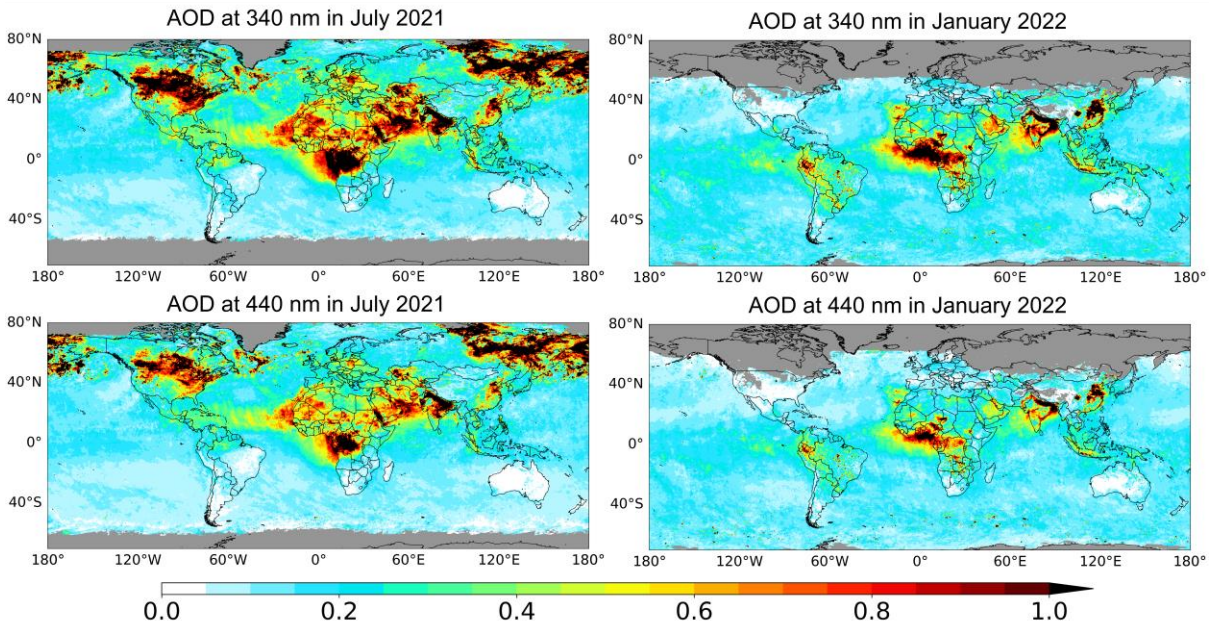

Figure S8. Spatial distribution of monthly AOD in July 2021 and January 2022 used in POMINO retrieval at 340 nm (first row) and 440 nm (second row). The regions in gray mean that there are no valid TROPOMI observations.

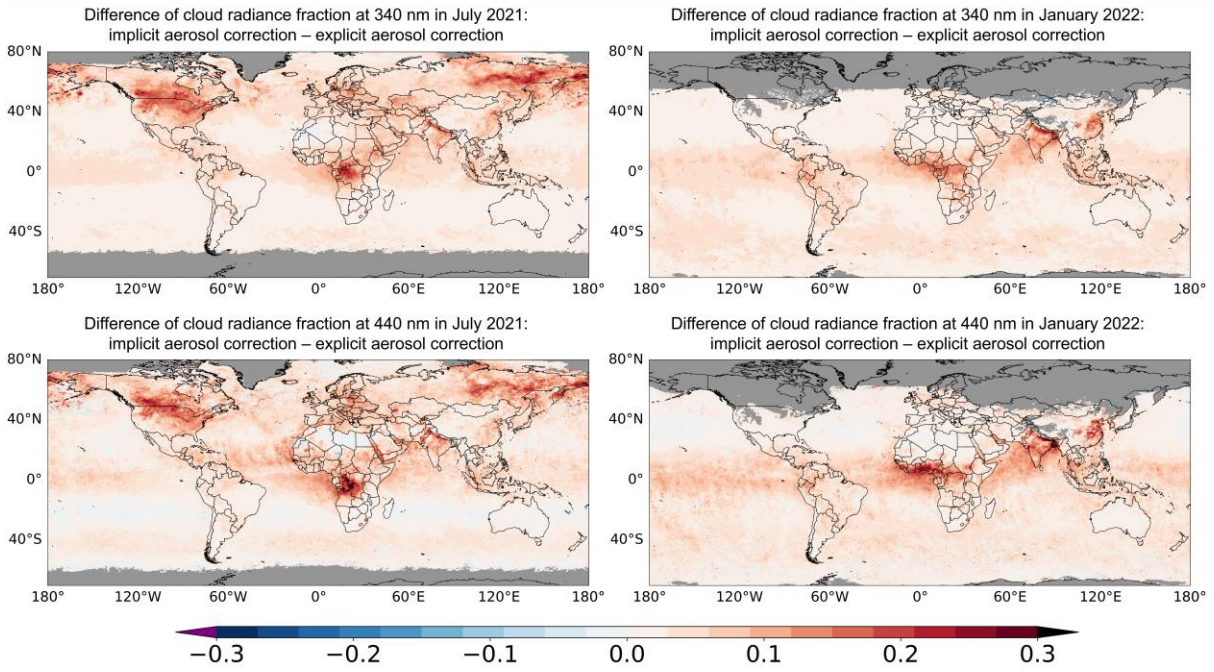

Figure S9. Absolute differences of cloud radiance fractions retrieved with implicit aerosol corrections (Cases "Fst_imaer" and "Nst_imaer") to those with explicit aerosol corrections (Case "Fst_ORcp" and POMINO NO_2) in July 2021 and January 2022 at 340 nm (first row) and 440 nm (440 nm). The regions in gray mean that there are no valid observations.

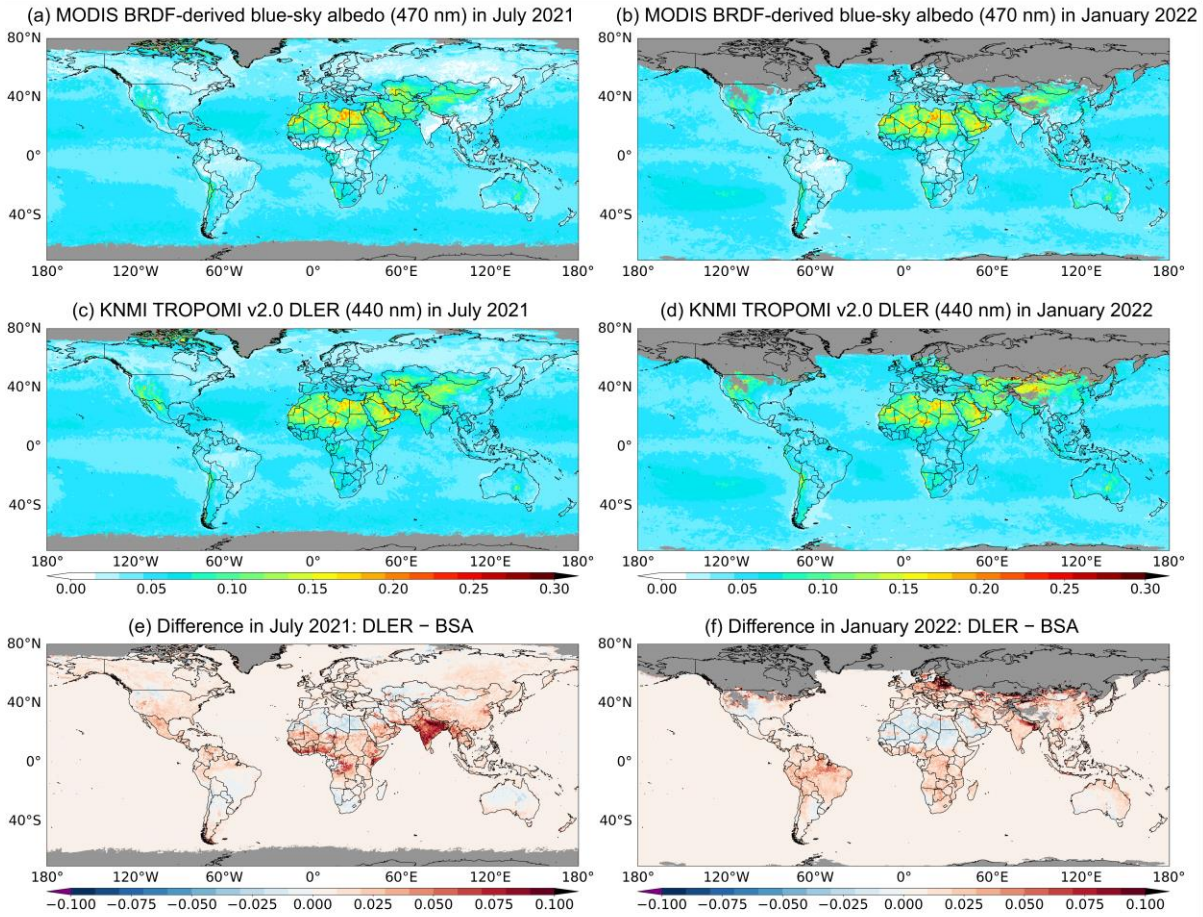

Figure S10. Spatial distribution of MODIS BRDF-derived blue-sky albedo (**a** and **b**), KNMI TROPOMI v2.0 DLER at 440 nm (**c** and **d**), and their absolute differences (**e** and **f**) in July 2021 and January 2022. The regions in gray mean that there are no valid observations.

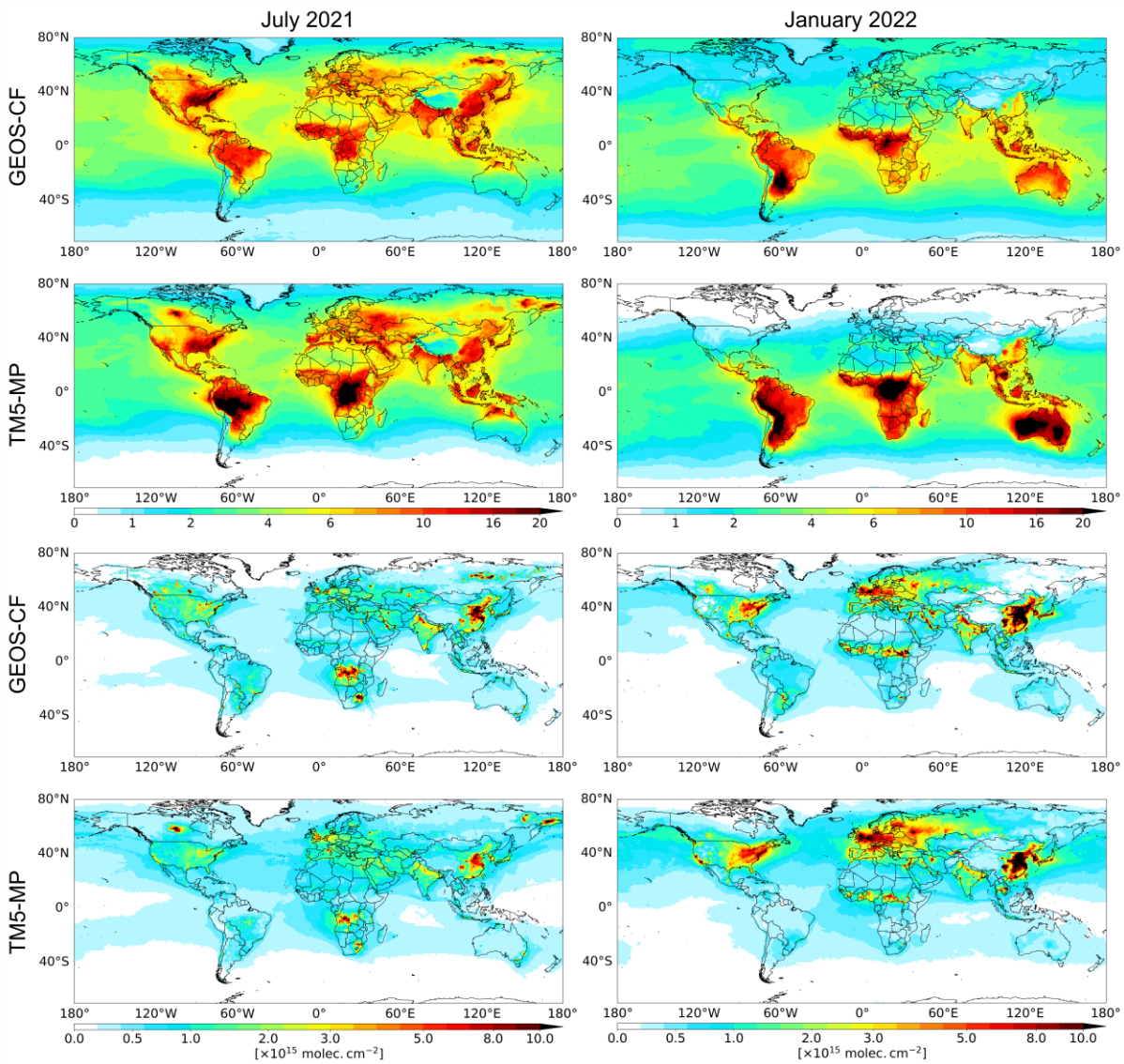

Figure S11. Spatial distribution of GEOS-CF and TM5-MP tropospheric HCHO (first and second rows) and NO_2 (third and fourth rows) VCDs in July 2021 and January 2022.

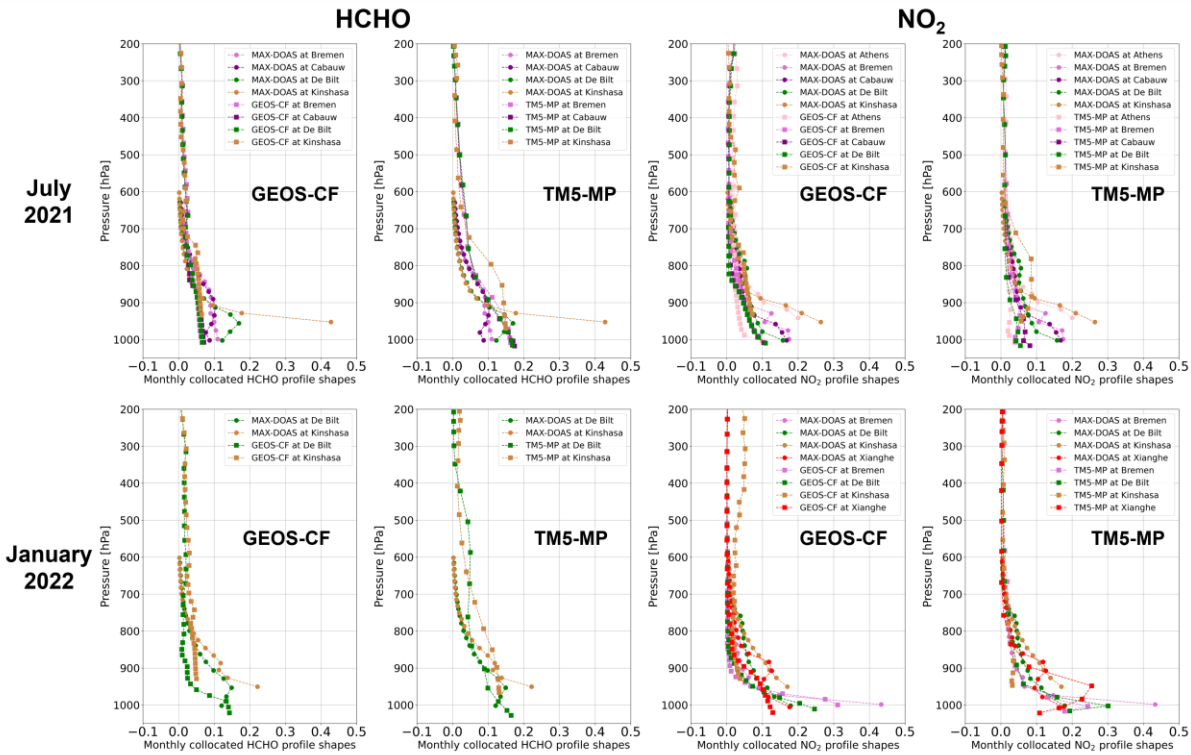

Figure S12. Comparisons of monthly collocated HCHO and NO_2 profile shapes between models (GEOS-CF or TM5-MP) and ground-based MAX-DOAS measurements in July 2021 and January 2022.

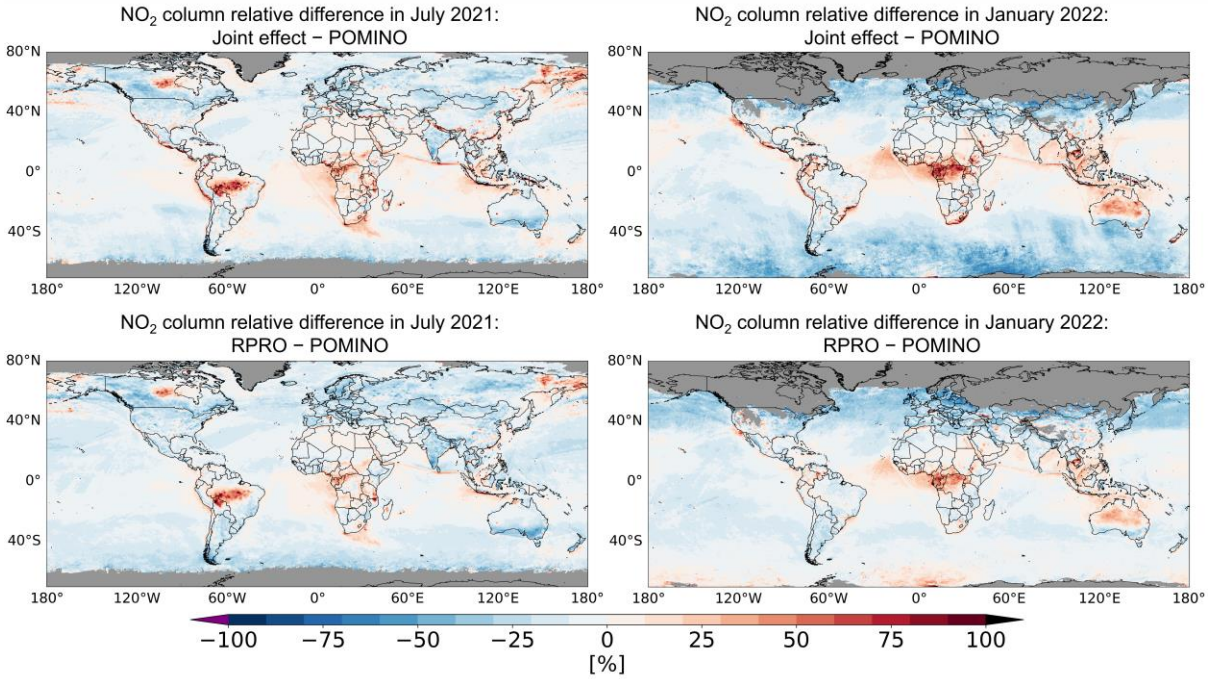

Figure S13. Relative differences of tropospheric NO_2 columns of sensitivity test "Nst_joint" (Case N4) to POMINO (first row) and those of RPRO to POMINO (second row) in July 2021 and January 2022. The regions in gray mean that there are no valid observations.

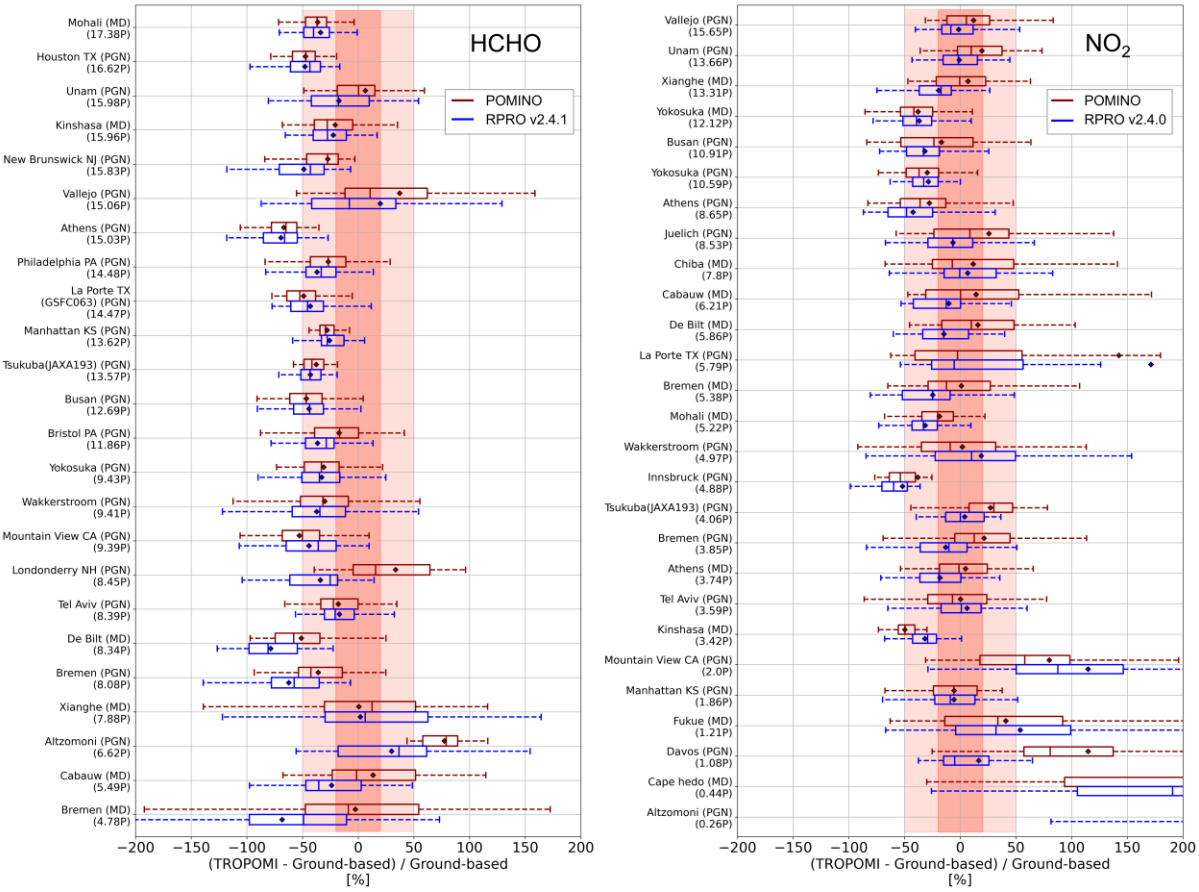

Figure S14. Box-and-whisker plots for the bias and spread of the relative difference of tropospheric HCHO (left) and NO_2 (right) columns between TROPOMI products (POMINO in red and RPRO in blue) and ground-based measurements. The box extends from the first quartile to the third quartile of the data, and the vertical solid line inside it represents the median difference. Mean difference is also shown by the diamond mark, and the whiskers extend from the box to the farthest data point lying within 1.5 times the inter-quartile range (IQR) from the box. The sites are ordered as a function of mean ground-based tropospheric columns in April, July, October 2021, and January 2022 (shown in the brackets in the unit of "P" as Pmolec.cm^{-2} = 1 × 10^{15} molec.cm^{-2}). "MD" represents MAX-DOAS sites and "PGN" represents PGN sites.

References

Chance, K. and Kurucz, R. L.: An improved high-resolution solar reference spectrum for earth's atmosphere measurements in the ultraviolet, visible, and near infrared, Journal of Quantitative Spectroscopy and Radiative Transfer, 111, 1289–1295, https://doi.org/10.1016/j.jqsrt.2010.01.036, 2010.

Chance, K. V. and Spurr, R. J. D.: Ring effect studies: Rayleigh scattering, including molecular parameters for rotational Raman scattering, and the Fraunhofer spectrum, Appl. Opt., AO, 36, 5224–5230, https://doi.org/10.1364/AO.36.005224, 1997.

Dee, D. P., Uppala, S. M., Simmons, A. J., Berrisford, P., Poli, P., Kobayashi, S., Andrae, U., Balmaseda, M. A., Balsamo, G., Bauer, P., Bechtold, P., Beljaars, A. C. M., van de Berg, L., Bidlot, J., Bormann, N., Delsol, C., Dragani, R., Fuentes, M., Geer, A. J., Haimberger, L., Healy, S. B., Hersbach, H., Hólm, E. V., Isaksen, L., Kållberg, P., Köhler, M., Matricardi, M., McNally, A. P., Monge-Sanz, B. M., Morcrette, J.-J., Park, B.-K., Peubey, C., de Rosnay, P., Tavolato, C., Thépaut, J.-N., and Vitart, F.: The ERA-Interim reanalysis: configuration and performance of the data assimilation system, Quarterly Journal of the Royal Meteorological Society, 137, 553–597, https://doi.org/10.1002/qj.828, 2011.

Eastham, S. D., Weisenstein, D. K., and Barrett, S. R. H.: Development and evaluation of the unified tropospheric–stratospheric chemistry extension (UCX) for the global chemistry-transport model GEOS-Chem, Atmospheric Environment, 89, 52–63, https://doi.org/10.1016/j.atmosenv.2014.02.001, 2014.

Fleischmann, O. C., Hartmann, M., Burrows, J. P., and Orphal, J.: New ultraviolet absorption cross-sections of BrO at atmospheric temperatures measured by time-windowing Fourier transform spectroscopy, Journal of Photochemistry and Photobiology A: Chemistry, 168, 117–132, https://doi.org/10.1016/j.jphotochem.2004.03.026, 2004.

Granier, C., Bessagnet, B., Bond, T., D'Angiola, A., Denier van der Gon, H., Frost, G. J., Heil, A., Kaiser, J. W., Kinne, S., Klimont, Z., Kloster, S., Lamarque, J.-F., Liousse, C., Masui, T., Meleux, F., Mieville, A., Ohara, T., Raut, J.-C., Riahi, K., Schultz, M. G., Smith, S. J., Thompson, A., van Aardenne, J., van der Werf, G. R., and van Vuuren, D. P.: Evolution of anthropogenic and biomass burning emissions of air pollutants at global and regional scales during the 1980–2010 period, Climatic Change, 109, 163, https://doi.org/10.1007/s10584-011-0154-1, 2011.

Guenther, A. B., Jiang, X., Heald, C. L., Sakulyanontvittaya, T., Duhl, T., Emmons, L. K., and Wang, X.: The Model of Emissions of Gases and Aerosols from Nature version 2.1 (MEGAN2.1): an extended and updated framework for modeling biogenic emissions, Geoscientific Model Development, 5, 1471–1492, https://doi.org/10.5194/gmd-5-1471-2012, 2012.

Holtslag, A. a. M. and Boville, B. A.: Local Versus Nonlocal Boundary-Layer Diffusion in a Global Climate Model, 1993.

Hudman, R. C., Moore, N. E., Mebust, A. K., Martin, R. V., Russell, A. R., Valin, L. C., and Cohen, R. C.: Steps towards a mechanistic model of global soil nitric oxide emissions: implementation and space based-constraints, Atmospheric Chemistry and Physics, 12, 7779–7795, https://doi.org/10.5194/acp-12-7779-2012, 2012.

Huijnen, V., Williams, J., van Weele, M., van Noije, T., Krol, M., Dentener, F., Segers, A., Houweling, S., Peters, W., de Laat, J., Boersma, F., Bergamaschi, P., van Velthoven, P., Le Sager, P., Eskes, H., Alkemade, F., Scheele, R., Nédélec, P., and Pätz, H.-W.: The global chemistry transport model TM5: description and evaluation of the

tropospheric chemistry version 3.0, Geoscientific Model Development, 3, 445–473, https://doi.org/10.5194/gmd-3-445-2010, 2010.

Janssens-Maenhout, G., Crippa, M., Guizzardi, D., Dentener, F., Muntean, M., Pouliot, G., Keating, T., Zhang, Q., Kurokawa, J., Wankmüller, R., Denier van der Gon, H., Kuenen, J. J. P., Klimont, Z., Frost, G., Darras, S., Koffi, B., and Li, M.: HTAP_v2.2: a mosaic of regional and global emission grid maps for 2008 and 2010 to study hemispheric transport of air pollution, Atmospheric Chemistry and Physics, 15, 11411–11432, https://doi.org/10.5194/acp-15-11411-2015, 2015.

J-F. Louis, M. Tiedtke, and J.-F. Geleyn: A short history of the PBL parameterization at ECMWF, in: Workshop on Planetary Boundary Layer parameterization, 25-27 November 1981, Workshop on Planetary Boundary Layer parameterization, 25-27 November 1981, Shinfield Park, Reading, 59–79, 1982.

Keller, C. A., Knowland, K. E., Duncan, B. N., Liu, J., Anderson, D. C., Das, S., Lucchesi, R. A., Lundgren, E. W., Nicely, J. M., Nielsen, E., Ott, L. E., Saunders, E., Strode, S. A., Wales, P. A., Jacob, D. J., and Pawson, S.: Description of the NASA GEOS Composition Forecast Modeling System GEOS-CF v1.0, Journal of Advances in Modeling Earth Systems, 13, e2020MS002413, https://doi.org/10.1029/2020MS002413, 2021.

Lin, S.-J.: A "Vertically Lagrangian" Finite-Volume Dynamical Core for Global Models, 2004.

Lock, A. P., Brown, A. R., Bush, M. R., Martin, G. M., and Smith, R. N. B.: A New Boundary Layer Mixing Scheme. Part I: Scheme Description and Single-Column Model Tests, 2000.

Marais, E. A. and Wiedinmyer, C.: Air Quality Impact of Diffuse and Inefficient Combustion Emissions in Africa (DICE-Africa), Environ. Sci. Technol., 50, 10739–10745, https://doi.org/10.1021/acs.est.6b02602, 2016.

Meijer, E. W., van Velthoven, P. F. J., Brunner, D. W., Huntrieser, H., and Kelder, H.: Improvement and evaluation of the parameterisation of nitrogen oxide production by lightning, Physics and Chemistry of the Earth, Part C: Solar, Terrestrial & Planetary Science, 26, 577–583, https://doi.org/10.1016/S1464-1917(01)00050-2, 2001.

Meller, R. and Moortgat, G. K.: Temperature dependence of the absorption cross sections of formaldehyde between 223 and 323 K in the wavelength range 225–375 nm, Journal of Geophysical Research: Atmospheres, 105, 7089–7101, https://doi.org/10.1029/1999JD901074, 2000.

Moorthi, S. and Suarez, M. J.: Relaxed Arakawa-Schubert. A Parameterization of Moist Convection for General Circulation Models, 1992.

Murray, L. T., Jacob, D. J., Logan, J. A., Hudman, R. C., and Koshak, W. J.: Optimized regional and interannual variability of lightning in a global chemical transport model constrained by LIS/OTD satellite data, Journal of Geophysical Research: Atmospheres, 117, https://doi.org/10.1029/2012JD017934, 2012.

Pope, R. M. and Fry, E. S.: Absorption spectrum (380–700 nm) of pure water. II. Integrating cavity measurements, Appl. Opt., AO, 36, 8710–8723, https://doi.org/10.1364/AO.36.008710, 1997.

Puķīte, J., Kühl, S., Deutschmann, T., Platt, U., and Wagner, T.: Extending differential optical absorption spectroscopy for limb measurements in the UV, Atmospheric Measurement Techniques, 3, 631–653, https://doi.org/10.5194/amt-3-631-2010, 2010.

Putman, W. M. and Lin, S.-J.: Finite-volume transport on various cubed-sphere grids, Journal of Computational Physics, 227, 55–78, https://doi.org/10.1016/j.jcp.2007.07.022, 2007.

Russell, G. L. and Lerner, J. A.: A New Finite-Differencing Scheme for the Tracer Transport Equation, 1981.

Schultz, M. G., Heil, A., Hoelzemann, J. J., Spessa, A., Thonicke, K., Goldammer, J. G., Held, A. C., Pereira, J. M. C., and van het Bolscher, M.: Global wildland fire emissions from 1960 to 2000, Global Biogeochemical Cycles, 22, https://doi.org/10.1029/2007GB003031, 2008.

Serdyuchenko, A., Gorshelev, V., Weber, M., Chehade, W., and Burrows, J. P.: High spectral resolution ozone absorption cross-sections – Part 2: Temperature dependence, Atmospheric Measurement Techniques, 7, 625–636, https://doi.org/10.5194/amt-7-625-2014, 2014.

Sindelarova, K., Granier, C., Bouarar, I., Guenther, A., Tilmes, S., Stavrakou, T., Müller, J.-F., Kuhn, U., Stefani, P., and Knorr, W.: Global data set of biogenic VOC emissions calculated by the MEGAN model over the last 30 years, Atmospheric Chemistry and Physics, 14, 9317–9341, https://doi.org/10.5194/acp-14-9317-2014, 2014.

Stettler, M. E. J., Eastham, S., and Barrett, S. R. H.: Air quality and public health impacts of UK airports. Part I: Emissions, Atmospheric Environment, 45, 5415–5424, https://doi.org/10.1016/j.atmosenv.2011.07.012, 2011.

Thalman, R. and Volkamer, R.: Temperature dependent absorption cross-sections of O2–O2 collision pairs between 340 and 630 nm and at atmospherically relevant pressure, Phys. Chem. Chem. Phys., 15, 15371–15381, https://doi.org/10.1039/C3CP50968K, 2013.

Van Geffen, J. H. G. M., Boersma, K. F., Van Roozendael, M., Hendrick, F., Mahieu, E., De Smedt, I., Sneep, M., and Veefkind, J. P.: Improved spectral fitting of nitrogen dioxide from OMI in the 405–465 nm window, Atmospheric Measurement Techniques, 8, 1685–1699, https://doi.org/10.5194/amt-8-1685-2015, 2015.

Vandaele, A. C., Hermans, C., Simon, P. C., Carleer, M., Colin, R., Fally, S., Mérienne, M. F., Jenouvrier, A., and Coquart, B.: Measurements of the NO2 absorption cross-section from 42 000 cm−1 to 10 000 cm−1 (238–1000 nm) at 220 K and 294 K, Journal of Quantitative Spectroscopy and Radiative Transfer, 59, 171–184, https://doi.org/10.1016/S0022-4073(97)00168-4, 1998.

van der Werf, G. R., Randerson, J. T., Giglio, L., Collatz, G. J., Mu, M., Kasibhatla, P. S., Morton, D. C., DeFries, R. S., Jin, Y., and van Leeuwen, T. T.: Global fire emissions and the contribution of deforestation, savanna, forest, agricultural, and peat fires (1997–2009), Atmospheric Chemistry and Physics, 10, 11707–11735, https://doi.org/10.5194/acp-10-11707-2010, 2010.

Williams, J. E., van Velthoven, P. F. J., and Brenninkmeijer, C. a. M.: Quantifying the uncertainty in simulating global tropospheric composition due to the variability in global emission estimates of Biogenic Volatile Organic Compounds, Atmospheric Chemistry and Physics, 13, 2857–2891, https://doi.org/10.5194/acp-13-2857-2013, 2013.

Williams, J. E., Boersma, K. F., Le Sager, P., and Verstraeten, W. W.: The high-resolution version of TM5-MP for optimized satellite retrievals: description and validation, Geoscientific Model Development, 10, 721–750, https://doi.org/10.5194/gmd-10-721-2017, 2017.

Zeng, G., Williams, J. E., Fisher, J. A., Emmons, L. K., Jones, N. B., Morgenstern, O., Robinson, J., Smale, D., Paton-Walsh, C., and Griffith, D. W. T.: Multi-model simulation of CO and HCHO in the Southern Hemisphere: comparison with observations and impact of biogenic emissions, Atmospheric Chemistry and Physics, 15, 7217–7245, https://doi.org/10.5194/acp-15-7217-2015, 2015.